BGSG

Volume 55

Research Paper

Correspondence to:
Aravani Foteini
faravani@geo.auth.gr

DOI number:
http://dx.doi.org/10.12681/bgsg.20755
Keywords:
epithermal veins, quartz, chalcedony, opal, FT-IR, fluid inclusions
Citation:
Aravani Foteini, Papadopoulou Lambrini, Melfos Vasileios, Soldatos Triantafillos, Zorba Triantafillia, Voudouris Panagiotis (2019), Mineralogical and Fluid Inclusion Study of Epithermal Type Veins Intruding the Volcanic Rocks of the Kornofolia Area, Evros, NE Greece. Bulletin Geological Society of Greece, 55, 202-222.
Publication History:
Received: 03/07/2019
Accepted: 16/11/2019
Accepted article online: 02/12/2019

The Editor wishes to thank two anonymous reviewers for their work with the scientific reviewing of the manuscript and Ms Erietta Vlachou for editorial assistance.

MINERALOGICAL AND FLUID INCLUSION STUDY OF EPITHERMAL TYPE VEINS INTRUDING THE VOLCANIC ROCKS OF THE KORNOFOLIA AREA, EVROS, NE GREECE.

Foteini Aravani [1*], Lambrini Papadopoulou [1], Vasileios Melfos [1], Triantafillos Soldatos [1], Triantafillia Zorba [2], Panagiotis Voudouris [3]

[1]Department of Mineralogy-Petrology-Economic Geology, School of Geology, Aristotle University of Thessaloniki, 54124 Thessaloniki, Greece,
faravani@geo.auth.gr lambrini@geo.auth.gr melfosv@geo.auth.gr soldatos@geo.auth.gr

[2]Solid State Physics Section, School of Physics, Aristotle University of Thessaloniki, Greece zorba@auth.gr

[3]Department of Mineralogy-Petrology, School of Geology and Geoenvironment, National and Kapodistrian University of Athens, 15784, Greece
voudouris@geol.uoa.gr

Abstract

The volcanic rocks of Kornofolia area, Evros, host a number of epithermal-type veins. The host rocks are Oligocene calc-alkaline andesites to rhyo-dacites. The andesites form hydrothermal breccias and show hydrothermal alteration. The veins comprise mainly silica polymorphs such as quartz, chalcedony and three types of opal (milky white, transparent and green). Amethyst also forms in veins at the same area. Apart from the silica polymorphs, the veins are accompanied by calcite and zeolites. The main aim of this study is the characterization of the silica polymorphs. Using FT-IR analyses, variations in the crystal structure of the three opals were recognized. The green opal is found to be more amorphous than the other two types. Fluid-inclusion measurements were performed in calcite and were compared with amethyst from previous studies. The T_h is

between 121-175 °C and the Te between -22.9 and -22.4 °C. The salinities range from 0.9 to 4.5 wt % NaCl equiv.

Keywords: *epithermal veins, quartz, chalcedony, opal, FT-IR, fluid inclusions*

Περίληψη

Τα ηφαιστειακά πετρώματα της περιοχής Κορνοφωλιά, Έβρου, φιλοξενούν μεγάλο αριθμό φλεβών επιθερμικού τύπου. Τα πετρώματα ξενιστές αποτελούνται από Ολιγοκαινικούς ασβεσταλκαλικούς ανδεσίτες έως ρυοδακίτες. Οι ανδεσίτες σχηματίζουν υδροθερμικά λατυποπαγή παρουσιάζοντας ενδείξεις υδροθερμικών εξαλλοιώσεων. Οι φλεβικές διεισδύσεις αποτελούνται κυρίως από πολύμορφα του πυριτίου όπως χαλαζία, χαλκηδόνιο και τρεις τύπους οπάλιου (γαλακτόχρωμο, διάφανο και πράσινο). Επίσης, στην ίδια περιοχή έχουν βρεθεί φλέβες που περιέχουν αμέθυστο. Εκτός από τα πολύμορφα του πυριτίου στις φλέβες υπάρχει ακόμη ασβεστίτης και ζεόλιθοι. Ο κύριος σκοπός της παρούσας εργασίας είναι ο χαρακτηρισμός των πολυμόρφων του πυριτίου. Με χρήση φασματοσκοπίας FT-IR αναγνωρίστηκαν διαφορές στην κρυσταλλική δομή των τριών οπαλίων. Ο πράσινος οπάλιος εμφανίζεται πιο άμορφος από τους άλλους δύο τύπους. Στον ασβεστίτη πραγματοποιήθηκαν αναλύσεις ρευστών εγκλεισμάτων οι οποίες συγκρίθηκαν με αντίστοιχες αναλύσεις αμέθυστου από προηγούμενες μελέτες. Η T_h βρίσκεται μεταξύ 121-175 °C και η Te μεταξύ -22.9 και -22.4 °C. Οι αλατότητες κυμαίνονται από 0.9 έως 4.5 wt % NaCl equiv.

Λέξεις κλειδιά: *επιθερμικές φλέβες, χαλαζίας, χαλκηδόνιος, οπάλιος, FT-IR, ρευστά εγκλείσματα*

1. Introduction

Silicon dioxide is a very common compound in Earth's crust. The crystal structure of silica depends on the temperature (T) and pressure (P) of crystallization, which result in the existence of many silica polymorphs. The most abundant silica polymorph is quartz. Polymorphs of low T-P of

crystallization are chalcedony and opal. Opal is usually more amorphous and contains water molecules, with the general chemical formula $SiO_2 \bullet nH_2O$. Some varieties of opal are considered precious, while the rest are classified as common. Gem quality opals display play-of-color, which is the result of diffraction from the regular three-dimensional structure arising from the regular packing of spaced array of regular spherical particles of silica (Sanders, 1964; Steward et al., 2010). Opals occur in cavities or fractures in volcanic or sedimentary environments. In volcanic environments opals form in open systems from precipitation of silica-rich solutions at relatively low temperatures during the latest hydrothermal stages of epithermal systems. These solutions usually affect the surrounding lithologies and cause extensive hydrothermal alterations forming new minerals in the fractures and cavities of the wall rocks (Gaillou et al., 2008).

The present work describes the mineralogical composition of epithermal-type veins which cut across the andesitic host rocks in Kornofolia area of Evros region, NE Greece and focuses on the silica minerals. In the same veins amethyst crystals occur which, have been studied by Melfos (2005) and Voudouris et al. (2018). This research provides new data about the forming conditions of these veins in Kornofolia expanding previous research. Focus is given to the various opal types, the alteration mineral assemblages and the formation conditions in terms of fluid inclusions.

2. Geological setting

The area of study is situated in north-eastern Greece where intensive Tertiary volcanic activity is evident throughout the region (Fig. 1). The Evros volcanic rocks can be found in the eastern parts of the Rhodope Massif (Bonev et al., 2010) and the Circum Rhodope belt (Meinhold & Kostopoulos, 2013). The magmatism is associated with sedimentary basins formed via detachment faulting and associated extensional collapse (Sokoutis et al., 1993; Dinter & Royden, 1993; Barr et al., 1999; Brun & Sokoutis, 2004; 2007; Kilias et al., 2013). The magmatism of Kornofolia consists of high-K calc-alkaline andesites to rhyo-dacites which have an Oligocene age, at 30.7 Ma, based on K/Ar dating (Christofides et al., 2004). They are intersected by many epithermal-type veins

and show indications of hydrothermal alteration. Voudouris et al. (2018) have conducted mineralogical, isotopic and fluid inclusion studies on the amethyst occurrences in similar veins from the same area. According to them, the amethyst co-exists in the veins with chalcedony and quartz along with smectite, zeolites (Ca-clinoptilolite and Ba-heulandite) and calcite.

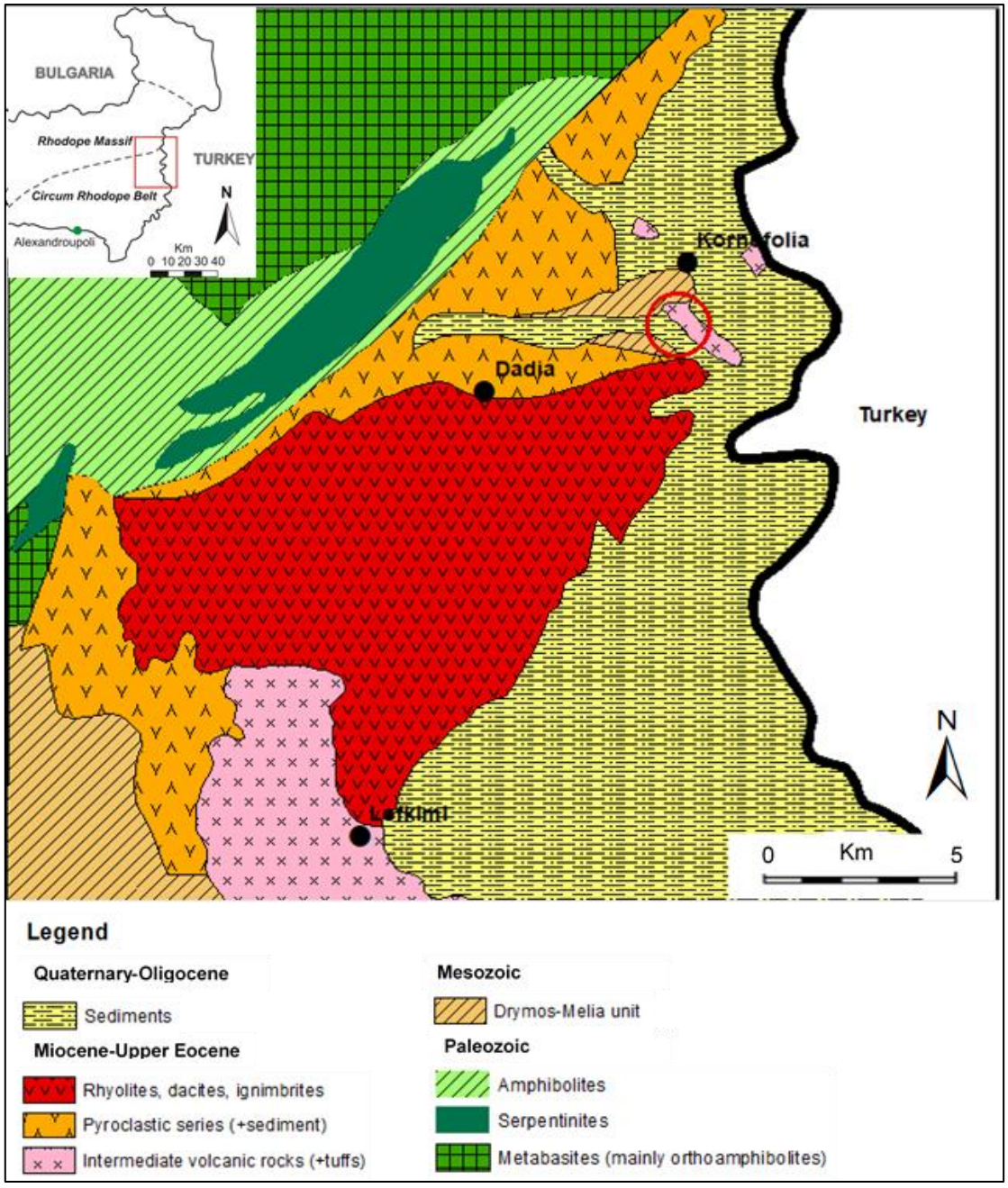

Fig. 1: Geological map of the broader Kornofolia area. The studied area is shown with a red rectangle (modified after Christofides et al., 2004).

3. Materials and methods

Ten polished-thin sections of both the andesitic host rock and the veins were studied by optical and scanning electron microscope in order to determine their mineralogical composition. The scanning electron microscope used was a JEOL JSM-6390LV type equipped with an energy dispersive spectrometer INCA 300, at the Laboratory of Scanning Electron Microscopy at Aristotle University of Thessaloniki. Analytical conditions were 20 kV operating voltage, 0.4 mA beam current, 80 s analysis time and ≈1 μm beam diameter.

Fourier Transform Infrared Spectroscopy (FT-IR) was utilized in order to determine the differences in the crystal structure of the silica minerals. The analysis was performed on five samples consisting of quartz, chalcedony, and three types of opal, namely a white, a transparent and a green opal, at the Solid State Physics Section, School of Physics, Aristotle University of Thessaloniki. Five compressed pellets were made of 2 mg of each sample mixed with 200 mg KBr. The range of the spectra recorded was in the mid-infrared (4000-400 cm^{-1}) in absorption mode. The data were collected on a Perkin-Elmer Spectrum 1000 FT-IR Spectrometer, accumulating 32 scans at a resolution of 4 cm^{-1}.

Fluid-inclusions measurements focused on calcite and quartz veins. Microthermometric data were obtained only from calcite, because quartz was free of inclusions probably due to post-entrapment processes. Freezing and heating runs were performed with a LINKAM THM-600/TMS 90 stage coupled on a Leitz SM-LUX-POL microscope at the Department of Mineralogy, Petrology and Economic Geology, Aristotle University of Thessaloniki, Greece. The stage was calibrated by using ice (H_2O) and organic reference substances with known melting points. The precision of the measurements was ±1 °C during heating and ±0.2 °C during freezing. The SoWat computer program by Driesner and Heinrich (2007) was used for the calculation of the fluid compositions in the system H_2O-NaCl. Densities and pressures were calculated from equations proposed by Driesner (2007).

4. Mineralogy

Based on petrographic observations the rocks under study are classified as andesites. The main mineral assemblage, emerging from microscopic observations and microanalysis, is zoned plagioclase (andesine to bytownite), magnesiohornblende and biotite (Tab. 1, Fig. 2 A, B, C, D). Hydrothermal brecciation occurs in places in the andesites (Sillitoe, 1985).

At the western part of the area, the andesite is fresh and the epithermal veins comprise mainly quartz, amethyst and chalcedony, while to the east, the matrix of the andesite is zeolitized and gradually it becomes silicified with veins comprising mostly three different silica polymorphs.

Three types of opal, in addition to quartz and chalcedony, were observed macroscopically, forming veins and binding the andesitic clasts of the breccia. On the basis of their colors, the opals are distinguished in three types: a white transparent type with a play-of-color effect, a milky-white type with a porcelain luster and a green type with a dull luster (Fig. 3A, B, C, D).

Quartz forms transparent white crystals with a length up to 3 cm (Fig. 3E). Chalcedony is white to grey with orange to brown tints displaying distinct zones of different color tones (Fig. 3F). Silica minerals in the veins are accompanied by calcite, zeolites (clinoptilolite and mordenite) and celadonite showing a lateral zonation (Fig. 2E, F, G, H).

Tab. 1: Representative chemical composition of plagioclase (Andesine, Bytownite), magnesiohornblende (Mg-Hbl) and biotite (Bi) of the fresh andesites.

	Andesine	**Bytownite**		**Mg-Hbl**			**Bi**
(wt %)	**1a-4**	**2a-7**	**(wt %)**	**1a-10**	**(wt %)**		**a-4**
SiO_2	61.63	48.44	SiO_2	47.67	SiO_2		41.96
Al_2O_3	24.15	33.42	TiO_2	0.66	TiO_2		3.92
FeO	0.28	1.09	Al_2O_3	7.70	Al_2O_3		14.22
MgO	0.04	0.00	FeO	14.33	FeO		14.97
CaO	7.16	15.37	MnO	0.00	MnO		0.37
Na_2O	6.24	1.77	MgO	14.96	MgO		15.36
K_2O	0.17	0.15	CaO	10.23	CaO		0.01
BaO	0.34	0.00	Na_2O	0.91	Na_2O		0.34
			K_2O	0.78	K_2O		8.78
			Cr_2O_3	0.04			
			NiO	0.83			
Total	100.01	100.24	Total	98.11	Total		99.93
Chemical formula (8 O)			**Chemical formula (23 O)**		**Chemical formula (22 O)**		
Si	2.734	2.207	Si	6.871	Si		5.894
Al	1.263	1.794	Al^{IV}	1.129	Al^{IV}		2.106
Fe^3	0.010	0.042	*T*	8.000	*Z*		8.000
Z	4.007	4.043	Al^{VI}	0.180	Al^{VI}		0.248
Mg	0.003	0.000	Ti	0.071	Ti		0.414
Ca	0.340	0.750	Fe^{3+}	0.655	Fe^{2+}		1.759
Na	0.537	0.156	Cr	0.004	Mn		0.044
K	0.010	0.009	Mg	3.214	Mg		3.216
Ba	0.006	0.000	Fe^{2+}	0.875	*Y*		5.681
X	0.895	0.915	Mn	0.000	Ca		0.002
Feldspar Structure			*C*	5.000	Na		0.093
Or (K+Ba)	1.73	0.95	Mg	0.000	K		1.573
Ab (Na)	59.95	17.08	Fe^{2+}	0.197	*X*		1.667
An (Ca+Mn+Mg)	38.31	81.97	Mn	0.000	$Mg/(Mg+Fe^{2+})$		0.647
			Ca	1.580			
			Na	0.223			
			B	2.000			
			Na	0.032			
			K	0.144			
			A	0.176			

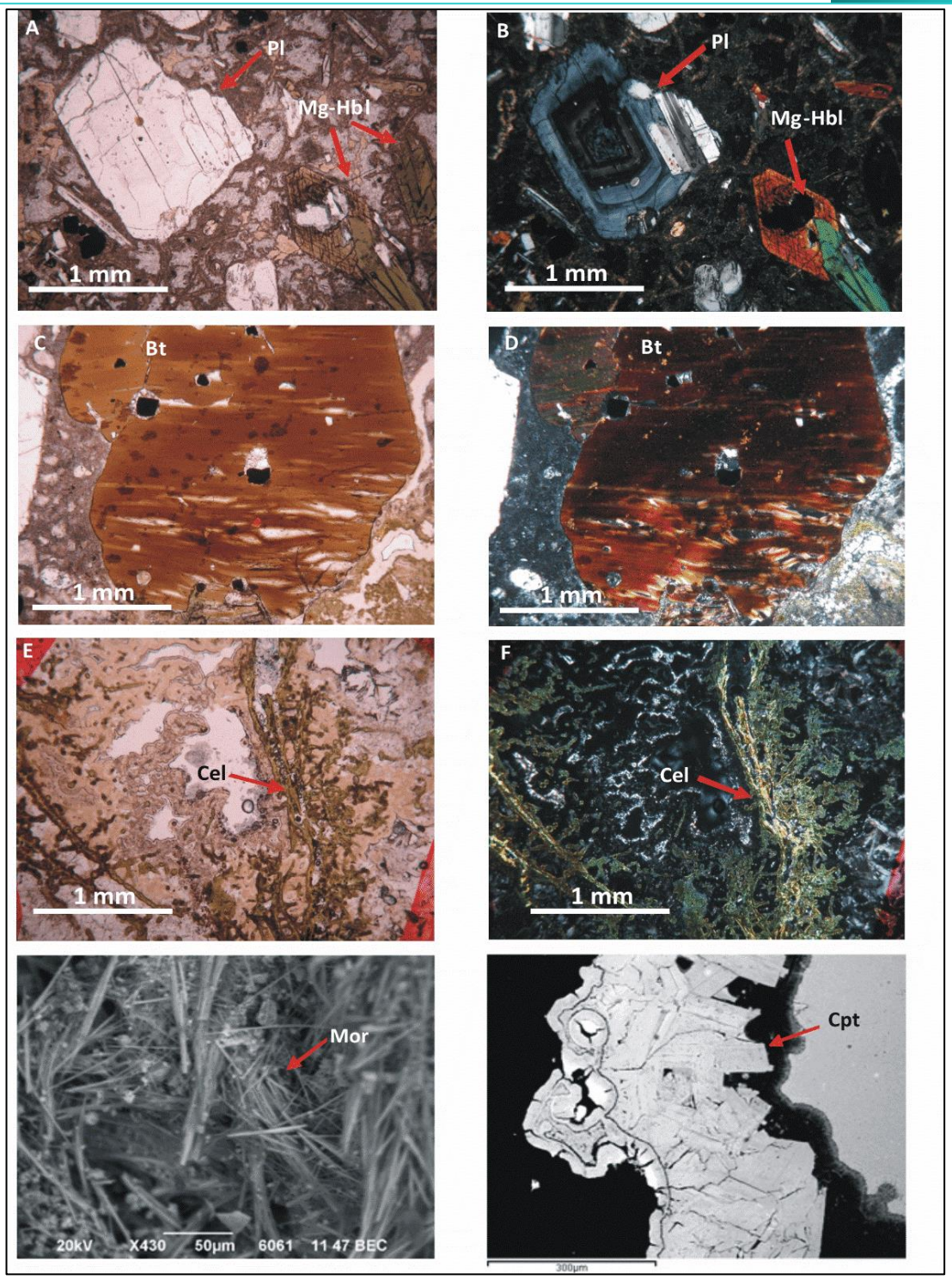

Fig. 2: Photomicrographs of the primary and secondary minerals of the fresh andesite and of the minerals accompanying the silica rich veins. A, B) Plagioclase (Pl) and magnesiohornblende (Mg-Hbl) in andesite parallel and crossed polars; C, D) Biotite (Bt) in thin section in //N and +N; E, F) Celadonite (Cel) in thin section in //N and +N G) Backscattered image of Mordenite (Mor) from SEM. H) backscattered image of Clinoptilolite (Cpt) from SEM.

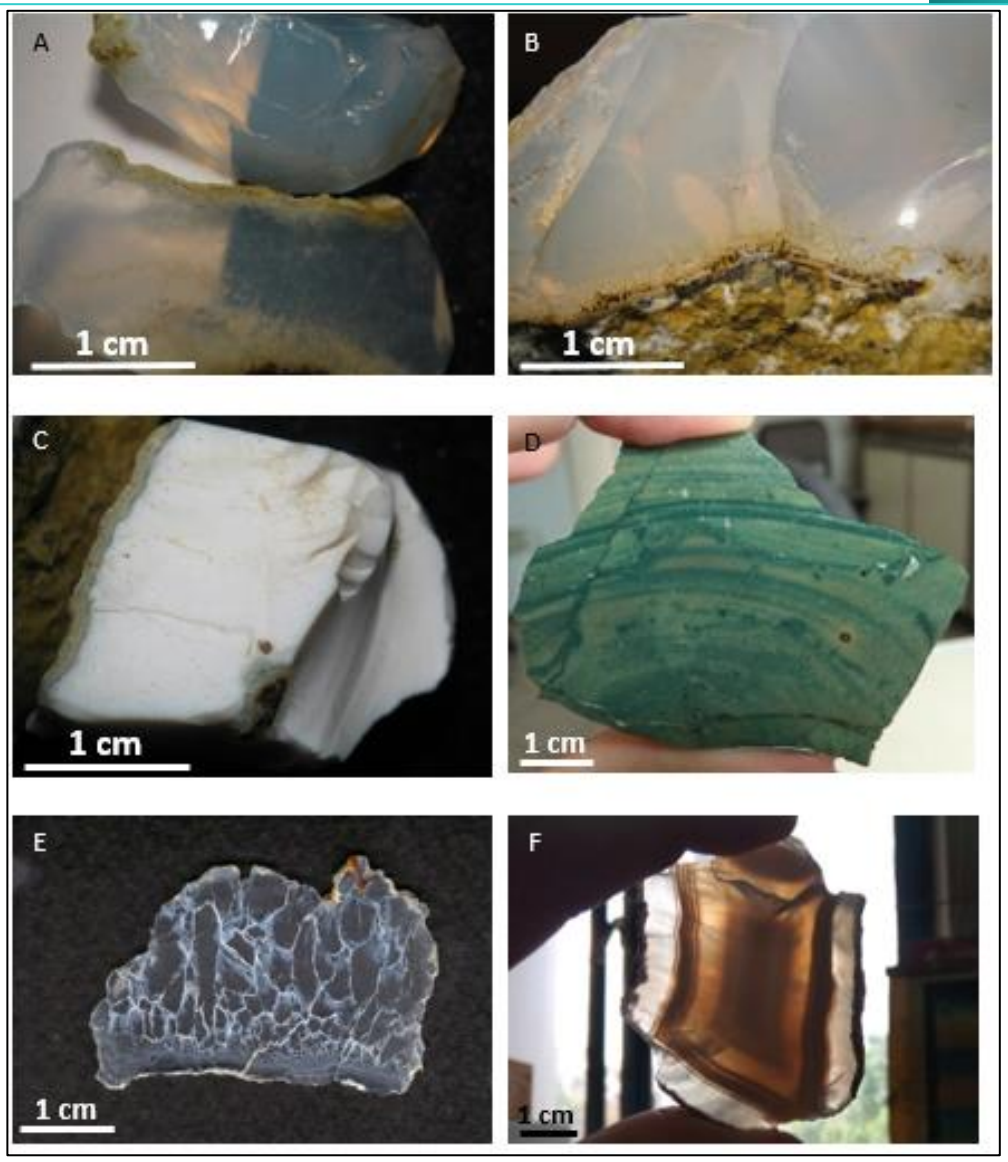

Fig. 3: Photographs of hand specimens of the various silica types at the Kornofolia area, including the three opal types (X6.5), quartz and chalcedony. A, B: transparent opal, C: white opal, D: green opal, E: quartz, F: chalcedony.

5. FT-IR results

The FT-IR spectra of all silica samples are characterized by a multi-component broad absorption band between approximately 3700-2900 cm^{-1}, centered at about 3430-3450 cm^{-1} (Fig. 4). These bands are attributed to the fundamental OH-stretching vibrations of hydrogen-bonded molecular water and Si-OH group (silanol) (Farmer, 1974). A peak at about 1630-1640 cm^{-1} due to the molecular water bending vibration is evident in all samples and is more intense in the three

opal samples (Farmer, 1974; Adamo et al., 2010). The peak at about 2360 cm^{-1} is attributed to ambient CO_2, therefore it must not be taken into account. In all the samples, the identifying peaks are between 1500 and 400 cm^{-1} (Fig. 4-8, marked with a thick red line). Three strong bands characterize all silicates with tetrahedrally-coordinated silicon related to the fundamental Si-O bond. These three bands are observed on the samples as follows: one at around 950-1300 cm^{-1} centered at 1100 cm^{-1}, one at 760-830 cm^{-1} centered at 790 cm^{-1} and one at 430-530 cm^{-1} centered at 470 cm^{-1} (Fig. 4) (Farmer, 1974; Adamo et al., 2010).

The quartz sample from the area of study (Qtz) was compared with a standard quartz sample (Qtz Std) from the Solid State Physics Section of Aristotle University of Thessaloniki (Fig. 5). The comparison between the two revealed that the spectra are identical. This confirms that the sample is actually quartz and not any other polymorph. The most distinguishing feature between quartz and the other silica polymorphs is the double peak at 780-790 cm^{-1} (Farmer, 1974). The chalcedony sample (Chalk) is calcite-contaminated probably due to the sampling process. In order to verify this, the chalcedony sample was compared with a standard calcite sample (Calcite Std) and a standard quartz sample (Qtz Std) from the Solid State Physics Section of Aristotle University of Thessaloniki (Fig. 6). Despite the contamination, the spectra analysis is thought to be reliable because none of the calcite peaks influence the chalcedony peaks. This comparison showed that the peaks at 1430 cm^{-1} and 876 cm^{-1} are due to the contamination and must not be taken into account. The chalcedony sample displays a double peak at 780-790cm^{-1} and generally coincides with the quartz spectrum.

The three opal types display the most significant variations in their spectra with the green opal type apparently differing from the other two. In contrast with the green opal (Op_g), the milky-white (Op_w) and the transparent opal (Op_p), display a strong peak at 622 cm^{-1} and a shoulder at 1200 cm^{-1} (Fig. 7). Green opal (Op_g) displays a strong peak at 694cm^{-1} that is an identifying trade of quartz (Fig. 8).

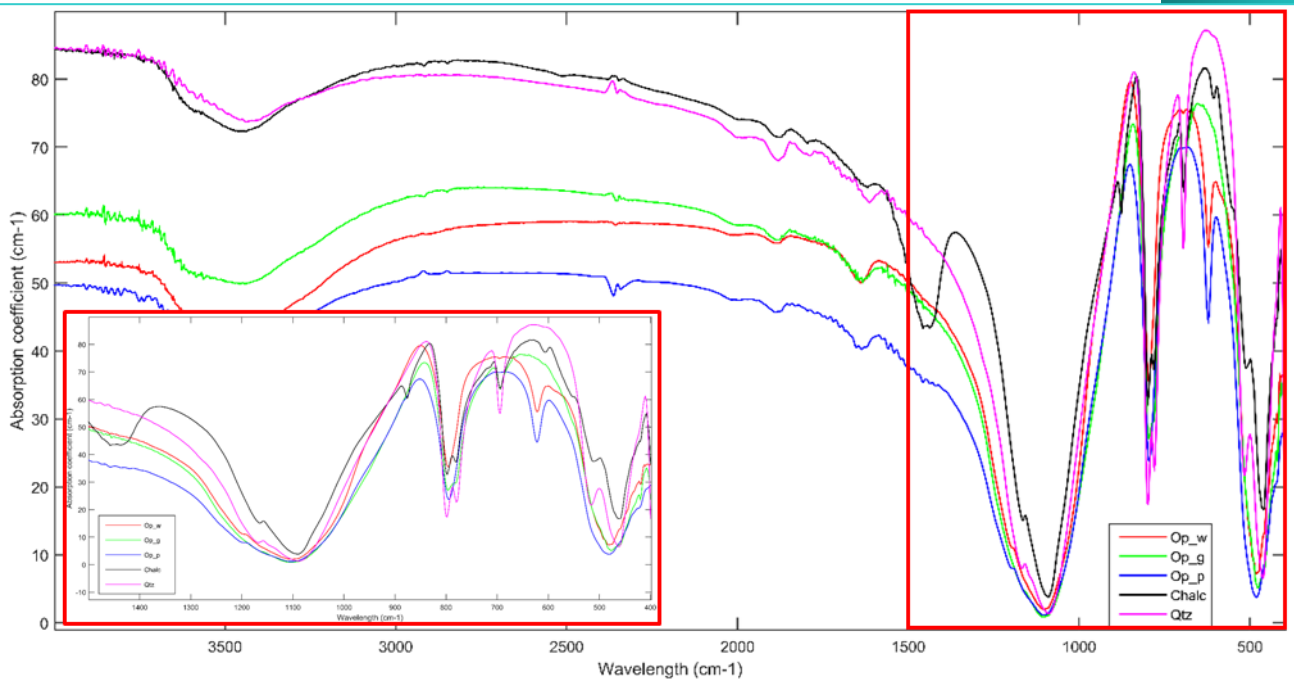

Fig. 4: FTIR spectra of all samples. Op_w: white opal, Op_g: green opal, Op_p: transparent opal, Chalc: chalcedony, Qtz: quartz. Area in thick red rectangle is magnified in the inset.

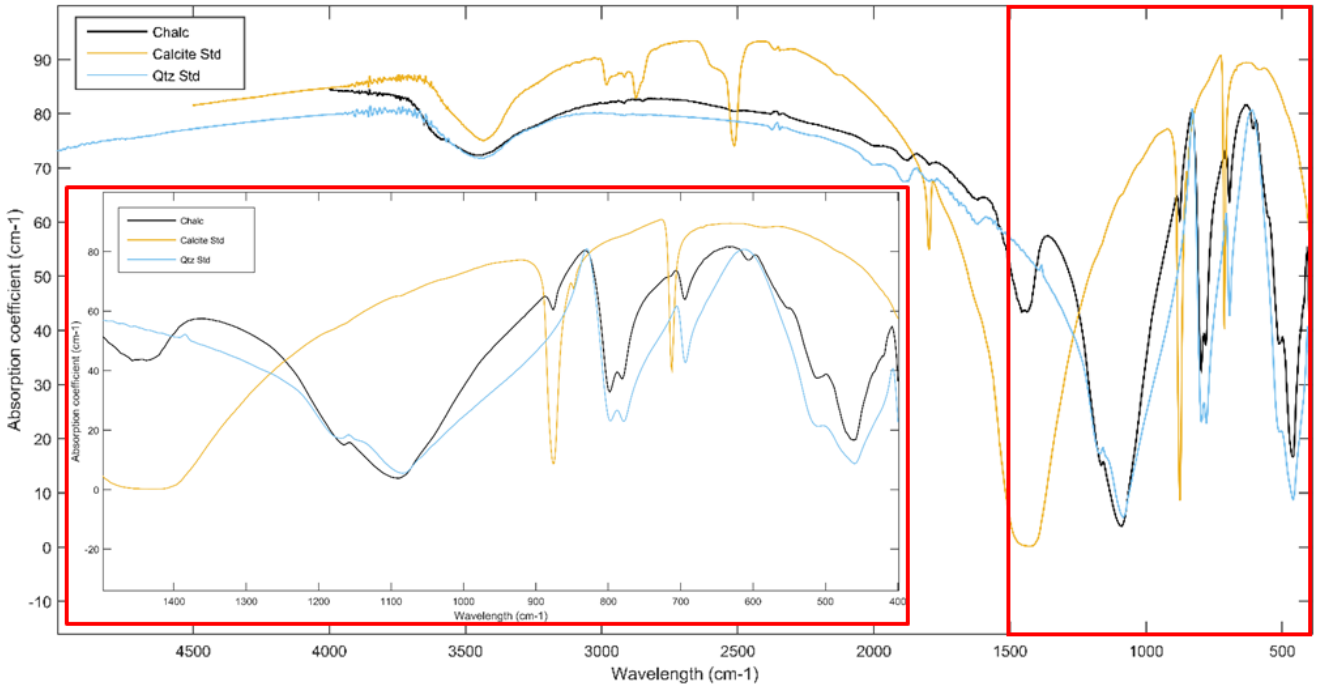

Fig. 5: FTIR spectra of quartz from the area of study (Qtz) with the standard quartz sample (Qtz Std). Area in thick red rectangle is magnified in the inset.

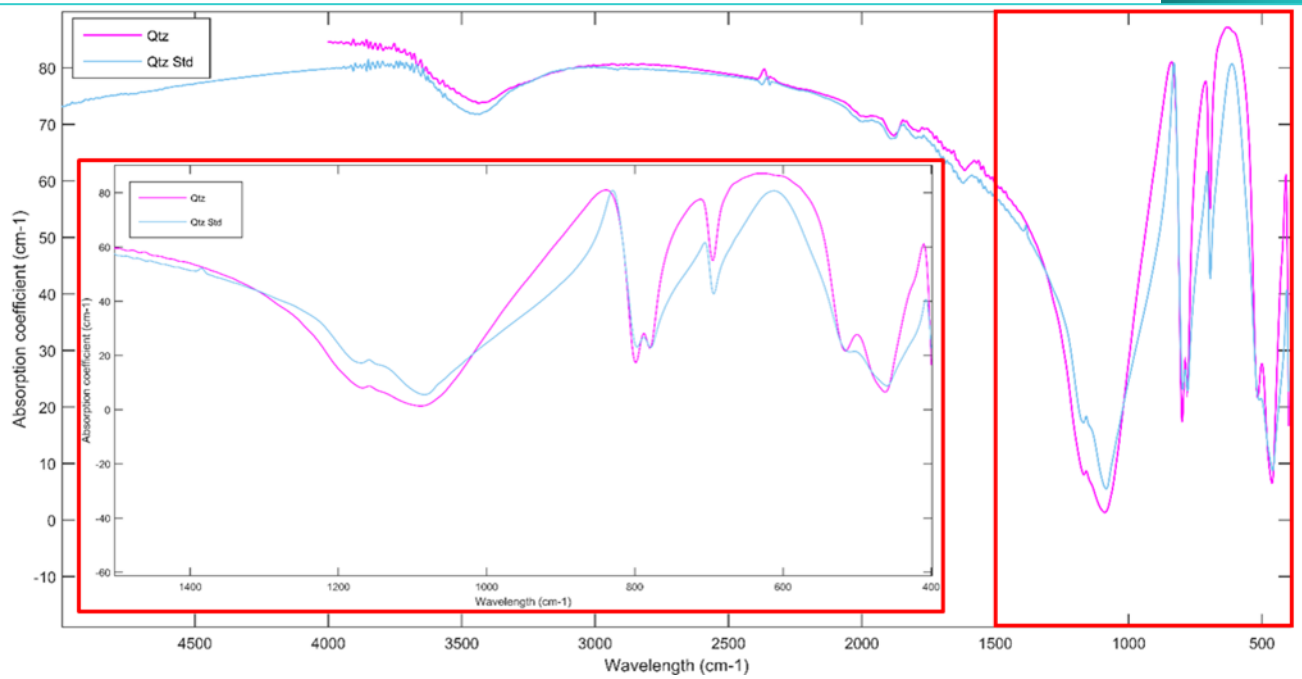

Fig. 6: FTIR spectra of chalcedony (Chalc) with quartz standard sample (Qtz Std) and calcite standard sample (Calcite Std). Area in thick red rectangle is magnified in the inset.

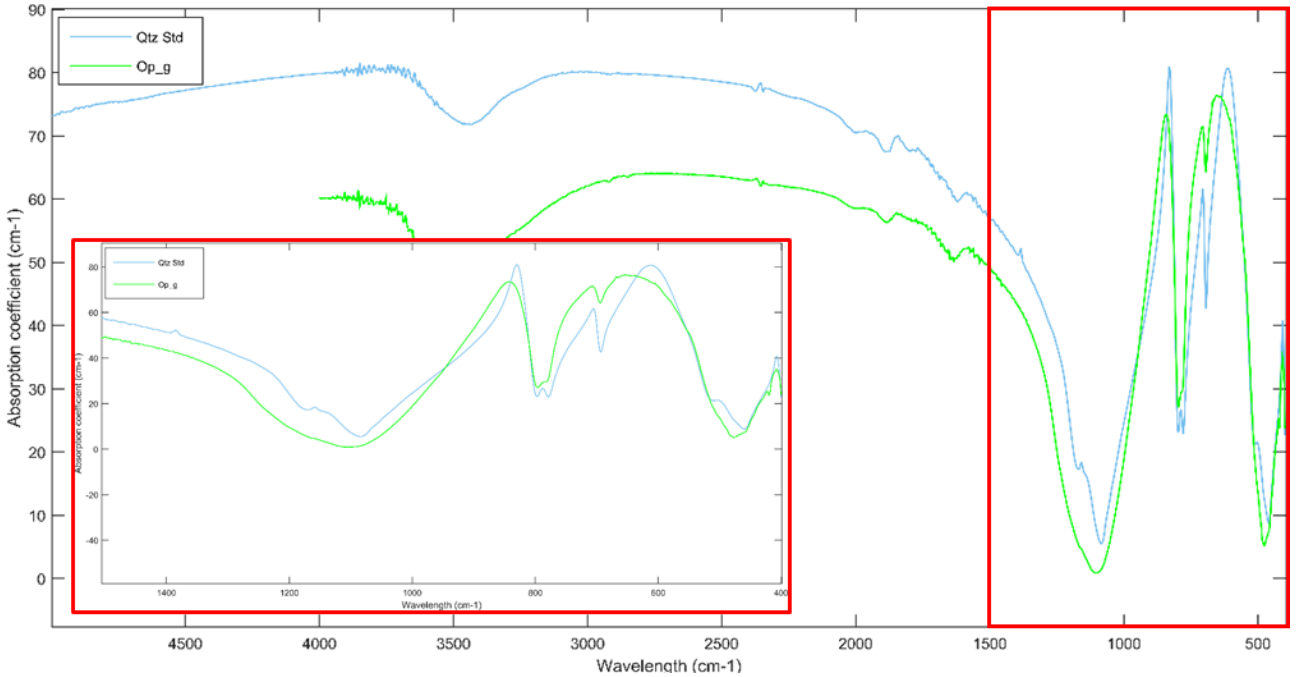

Fig. 7: FTIR spectra of the three opal samples. Op_w: white opal, Op_g: green opal, Op_p: transparent opal. Area in thick red rectangle is magnified in the inset.

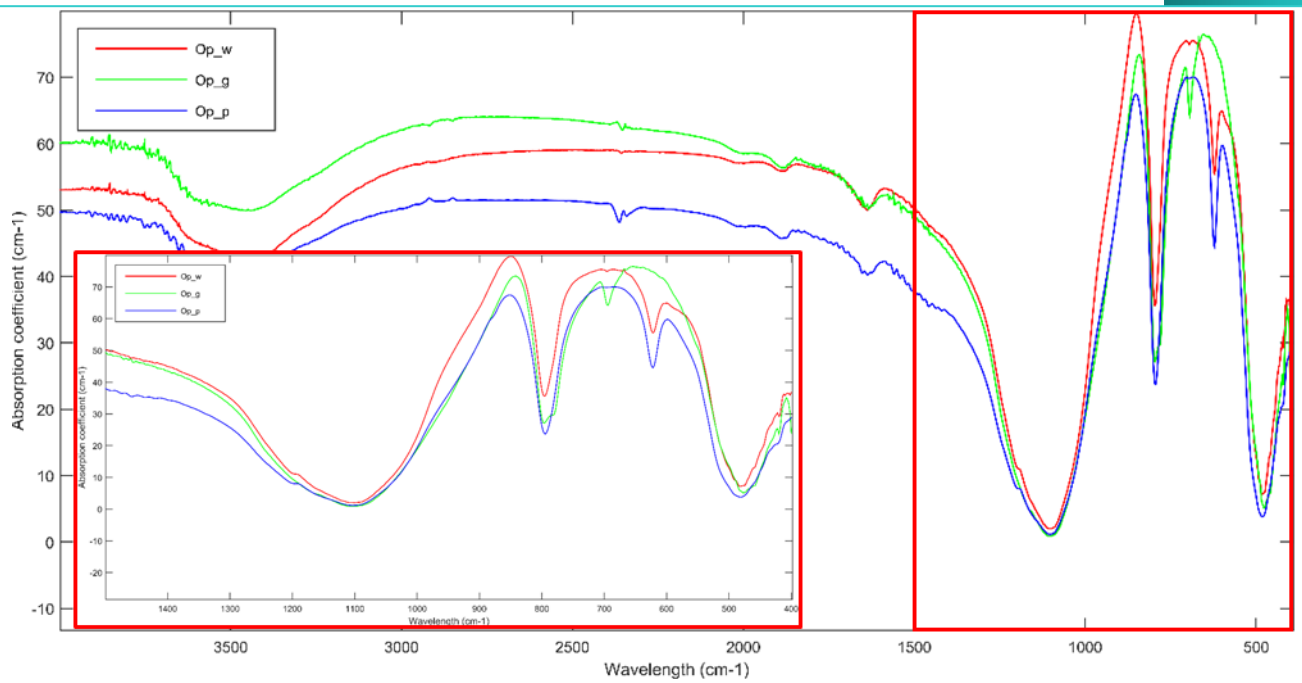

Fig. 8: FTIR spectra of green opal sample (Op_g) with quartz standard sample (Qtz Std). Area in thick red rectangle is magnified in the inset.

6. Fluid Inclusions

Only one type of fluid inclusions with two aqueous phases, a liquid and a vapor, at room temperature, were identified in the calcite crystals (Fig. 9a, b). The studied inclusions are considered to be primary in origin, on the basis of the criteria established by Roedder (1984) and Goldstein and Reynolds (1994). These criteria include similarities in shape, size and liquid to vapor ratios. The inclusions have a size ranging from 8 to 60 μm and constant liquid/vapor ratio, ~5-10 volume % vapor. Post-entrapment modifications, including necking down and leakage, affected most of the fluid inclusions (Fig. 9a), producing a significant amount of vapor, while liquid escaped along micro-cracks of calcite due to mechanical intracrystalline strain (Audétat and Günther, 1999; Tarantola et al., 2010). Freezing of the fluid inclusions in calcite revealed eutectic temperatures (T_e) between −22.9 and −22.4 °C, indicating that the dissolved salt is dominated only by NaCl (Shepherd et al., 1985). The temperatures of final ice melting range from −2.7 to −0.5 °C indicating salinities of 0.9 to 4.5 wt % NaCl equiv. (Bodnar, 2003). Homogenization temperatures range from 121 to 175 °C,

with a distinct peak at 140 °C (Fig. 10). All measurements and calculations of temperature, salinity, density and pressure are given in Table 2.

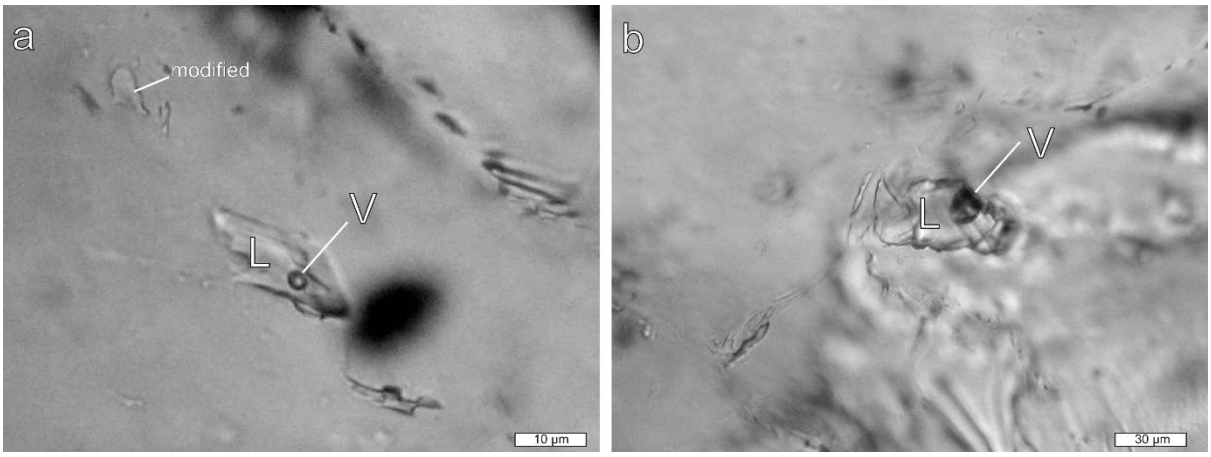

Fig. 9: Photomicrographs of fluid inclusions from the studied calcite under plane-polarized light. (a) Primary two-phase liquid-rich fluid inclusion and a modified inclusion which contains only vapor due to liquid leaking; (b) Primary two-phase liquid-rich fluid inclusion. L liquid phase, V vapor phase.

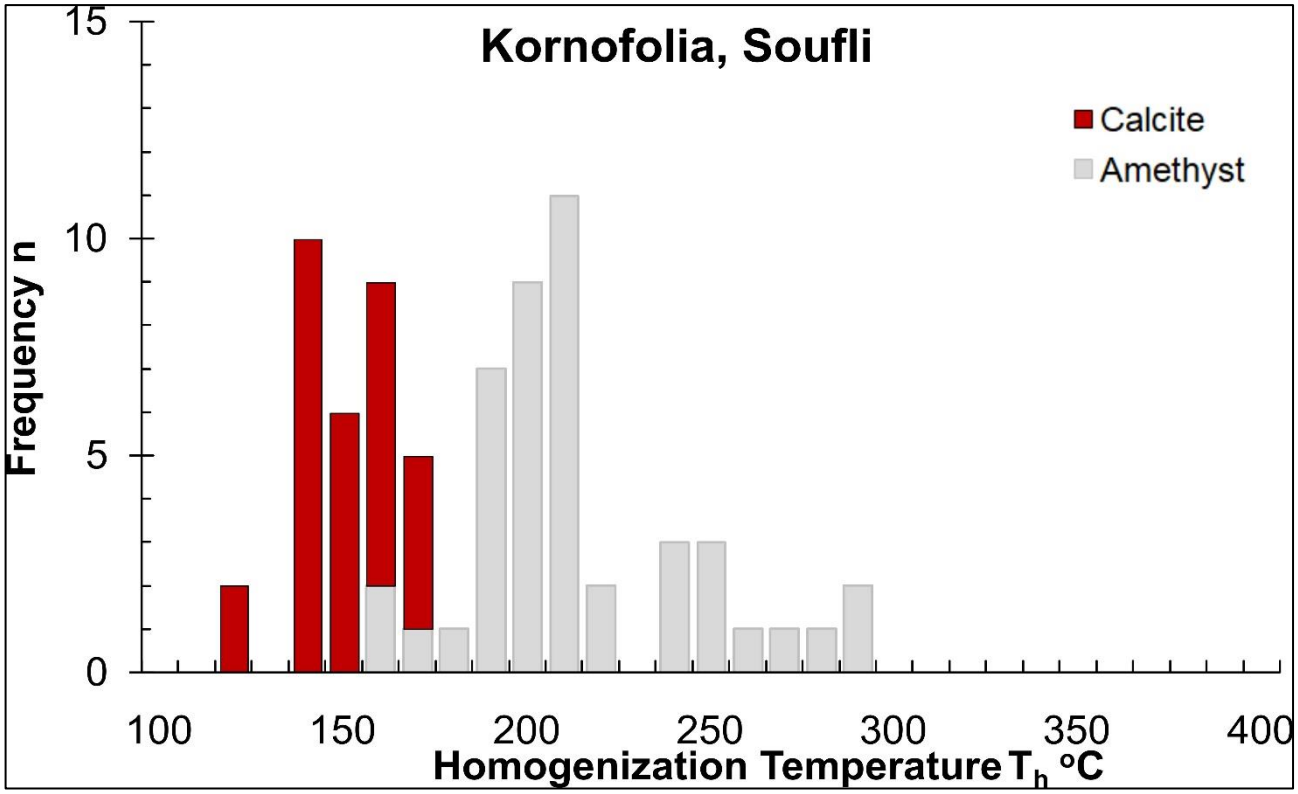

Fig. 10: Distribution of the homogenization temperatures of fluid inclusions in calcite (this study) from Kornofolia. Homogenization temperatures in amethysts obtained from Voudouris et al. (2018), are also included for comparison.

Tab. 2: Microthermometric results with salinities, densities and calculated minimum trapping pressures of the fluid inclusions in calcite from the Kornofolia epithermal veins. Fluid densities and minimum trapping pressures were calculated using the equation of state developed by Driesner (2007) and Driesner and Heinrich (2007), and implemented by the SoWat software (http://www.geopetro.ethz.ch/people/td/sowat).

T_h: homogenization temperature; T_m: melting temperature of ice; Sal: salinity; d: density; P: pressure.

T_h (°C)	T_m (°C)	Sal (wt % NaCl equiv)	d (g/cm^3)	P (bars)
146	-0.7	1.22	0.93	4.2
157	-1.0	1.74	0.92	5.7
162	-1.2	2.07	0.92	6.4
170	-0.9	1.57	0.91	7.8
159	-0.8	1.40	0.92	6.0
168	-1.7	2.90	0.92	7.4
163	-1.9	3.23	0.93	6.5
175	-1.0	1.73	0.91	8.8
149	-0.5	0.88	0.92	4.6
147	-2.5	4.18	0.95	4.3
147	-1.1	1.90	0.93	4.3
149	-1.8	3.06	0.94	4.5
142	-1.9	3.23	0.95	3.7
121	-1.4	2.02	0.96	2.0
144	-1.5	2.57	0.94	4.0
149	-1.5	2.57	0.94	4.6
155	-2.7	4.49	0.95	5.3
157	-2.1	3.55	0.94	5.6
148	-0.8	1.40	0.93	4.5
161	-1.0	1.74	0.92	6.3
167	-0.7	1.22	0.91	7.3
123	-	-	-	-
148	-	-	-	-
153	-	-	-	-
158	-	-	-	-
173	-	-	-	-
160	-	-	-	-
169	-	-	-	-
171	-	-	-	-

7. Discussion – Conclusions

The andesite of Kornofolia area is brecciated and the main mineral assemblage is zoned plagioclase (andesine to bytownite), magnesiohornblende, biotite and celadonite. Andesite is intersected by a number of epithermal-type veins. The veins represent hydrothermal fluids which also fill the spaces between the clasts of the andesite breccia. The most abundant minerals in the veins are silica polymorphs with minor calcite and zeolites (mordenite and clinoptilolite). The silica polymorphs include three types of opal, quartz and chalcedony. Especially the transparent opal (Op_p) that displays play-of-colors is characterized as precious (Farmer, 1974; Adamo, 2010). The samples Op_g and Op_w are characterized as common. The succession of the mineral phases in the veins, from the outside inwards, is celadonite - euhedral clinoptilolite - white opal - chalcedony – quartz and/or amethyst and mordenite. Calcite appears to be the last mineral that precipitates from the hydrothermal solutions.

The spectra acquired by FT-IR spectroscopy displayed significant differences among the three opal types. The strong peak at 622 cm^{-1} and the shoulder at 1200 cm^{-1} in the spectra of white (Op_w) and transparent opal (Op_p) characterize the spectrum of α-cristobalite and indicates that their crystal structure is similar to relatively well-ordered α-cristobalite, with minor evidence of tridymite (Farmer, 1974). Therefore, they are characterized as opal-C (Farmer, 1974; Adamo et al., 2010). The lack of those features in the spectrum of green opal indicates that it is more amorphous which according to Farmer (1974) could be characterized either as opal-CT or opal-A. The difference between opal-CT and opal-A is the shift towards higher or lower values respectively, of the three bands that characterize the silica polymorphs (Adamo et al, 2010). The shift of the bands on the green opal spectrum is from 1100 cm^{-1} to 1106 cm^{-1}, from 790 cm^{-1} to 796 cm^{-1} and from 470 cm^{-1} to 478 cm^{-1}. These shifts show that the crystal structure of the green opal is that of disordered α-cristobalite with α-tridymite-type stacking. Therefore, it is characterized as opal-CT (Farmer, 1974; Adamo et al., 2010).

Microthermometric data of the fluid inclusions in calcite from Kornofolia demonstrate the evolution of the hydrothermal fluid phase responsible for calcite formation and its relation with the amethyst formation studied by Voudouris et al. (2018). The plots of T_h versus salinity (Fig. 11) show low salinities (0.9 to 4.5 wt% NaCl equiv.) at low temperatures of 121 to 175 °C, with a peak at 140 °C. Stratigraphic reconstruction in the Kornofolia volcanic field does not allow a precise determination of the depth of calcite formation.

However, the pressure correction is insignificant by comparison to other shallow volcanic environments (e.g., Bodnar et al., 1985). In this case, the measured T_h corresponds to the temperature, which is very close to that of the calcite formation. The trend of the fluid inclusions in calcite and amethyst from higher to lower temperatures and salinities (Fig. 11) indicates a dilution process due to mixing of moderately saline hydrothermal fluids with low-temperature and low-salinity fluids, as it is suggested by Hedenquist (1991). The evolution of the fluids from the amethyst formation to the calcite crystallization shows a continuous process from high to low T_h with decreasing of salinities (Fig. 11).

The trapping pressures of the fluid inclusions in Kornofolia were calculated using the SoWat software (Driesner, 2007; Driesner and Heinrich, 2007), assuming that the inclusions were trapped in the NaCl-H_2O system, at a very shallow environment. The calculated minimum trapping pressures in the calcite vary between 3.74 and 6.52 bars, indicating a maximum depth of calcite formation between 15 and 25 m at hydrostatic conditions. The estimated densities of the hydrothermal fluids are >0.91 g/cm^3.

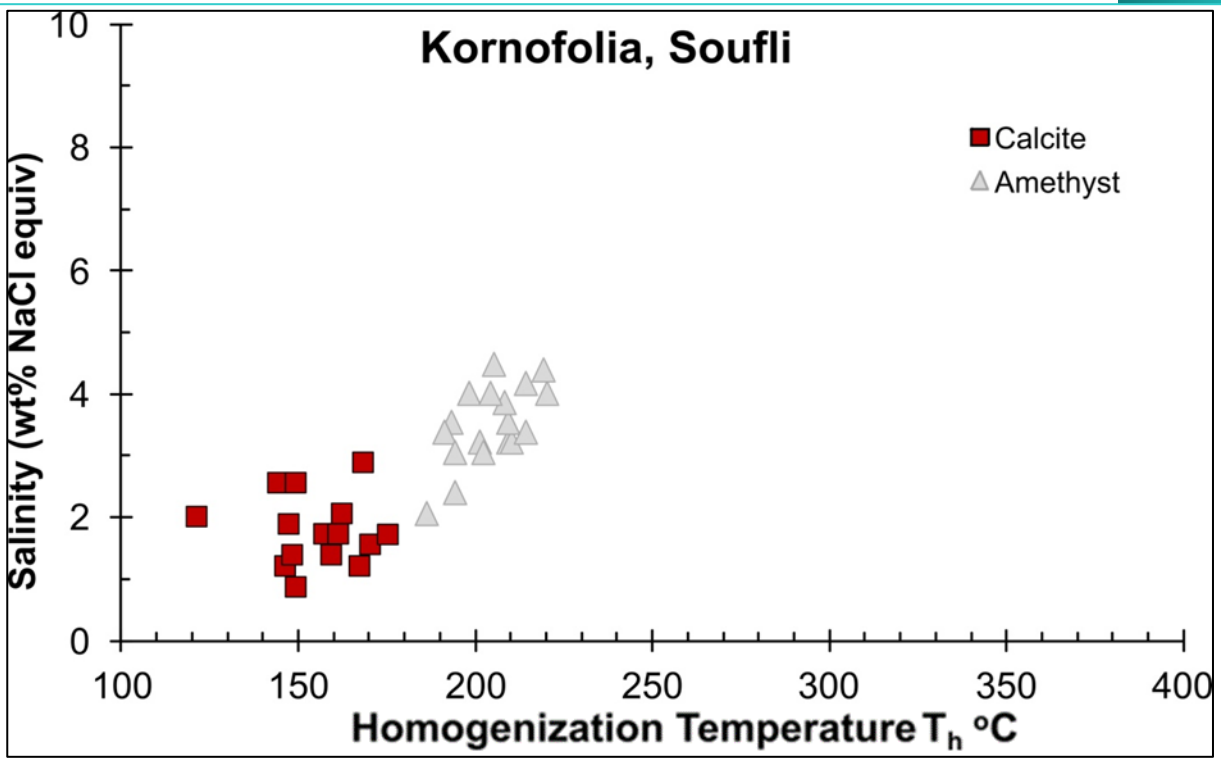

Fig. 11: Homogenization temperatures versus salinity diagram of fluid inclusions from calcite (this study) and amethyst (Voudouris et al., 2018) from Kornofolia area.

8. References

Adamo, I., Ghisoli, C. & Caucia, F., 2010. A contribution to the study of FTIR spectra of opals. *N. Jb. Miner. Abh.* 187/1, 63-68

Audétat, A., Günther, D., 1999. Mobility and H2O loss from fluid inclusions in natural quartz crystals. *Contrib. Mineral. Petrol.*, 137, 1–14.

Barr, S.R., Temperley, S., Tarney, J., 1999. Lateral growth of the continental crust through deep level subduction-accretion: a reevaluation of central Greek Rhodope. *Lithos*, 46, 69–94.

Bodnar, R.J., 2003. Introduction to fluid inclusions. In Fluid Inclusions: Analysis and Interpretation; Samson, I.M., Anderson, A.J., Marshall, D.D., Eds.; SEPM Short Course; *Society for Sedimentary Geology: Broken Arrow, OK, USA, Volume* 32, 1–8.

Bodnar, R.J., Reynolds, T.J., Kuehn, C.A., 1985. Fluid-Inclusion systematics in epithermal systems. *Rev. Econ. Geol.* 2, 73–97.

Bonev, N., Marchev, P., Ovtcharova, M., Moritz, R. and Ulianov, A., 2010. U-Pb LA-ICP/MS zircon geochronology of metamorphic basement and Oligocene volcanic rocks from the SE Rhodopes: inferences for the geological history of the Eastern Rhodope crystalline basement. *National Conference of the Bulgarian Geological Society, Bulgarian Geological Society, Sofia*. 115-116.

Brun, J. P., & Sokoutis, D., 2004. North Aegean extension: from the Rhodope core complex to Neogene basins. *In Proceedings of the 5th International Symposium of Eastern Mediterranean Geology, Thessaloniki, Greece* Vol. 1, 49-52.

Brun, J. P., & Sokoutis, D., 2007. Kinematics of the southern Rhodope core complex (North Greece). *International Journal of Earth Sciences*, 96(6), 1079-1099.

Christofides, G., Pecskay, Z., Eleftheriadis, G., Soldatos, T., & Koroneos, A., 2004. The Tertiary Evros volcanic rocks (Thrace, northeastern Greece): Petrology and K/Ar geochronology. Geologica Carpathica-Bratislava, 55(5), 397-410.

Dinter, D.A. & Royden, L., 1993. Late Cenozoic extension in northeastern Greece: Strymon Valley detachment system and Rhodope metamorphic core complex. *Geology*, 21 (1), 45-48.

Driesner, T., 2007. The system H2O–NaCl. Part II: Correlations for molar volume, enthalpy, and isobaric heat capacity from 0 to 1000 C, 1 to 5000 bar, and 0 to 1 XNaCl. *Geochim. Cosmochim. Acta* 71, 4902-4919.

Driesner, T., and Heinrich, C.A., 2007. The system H2O-NaCl. I. Correlations for molar volume, enthalpy, and isobaric heat capacity from 0 to 1000 degrees C, 1 to 5000 bar, and 0 to 1 X-NaCl. *Geoch. Cosmoch. Acta*, 71, 4880–4901.

Farmer, V.C., 1974. The infrared spectra of minerals. Silica, the three-dimentional silicates, borosilicates and beryllium silicates. *Mineralogical society monograph 4. Moenke H.H.W*, 16, 365-370.

Gaillou, E., Delaunay, A., Rondeau, B., Bouhnik-le-Coz, M., Fritsch, E., Cornen, G., & Monnier, C., 2008. The geochemistry of gem opals as evidence of their origin. *Ore Geology Reviews*, 34(1-2), 113-126.

Goldstein, R.H., Reynolds, T.J., 1994. Systematics of Fluid Inclusions in Diagenetic Minerals, *SEPM Short Course, Society for Sedimentary Geology: Broken Arrow, OK, USA*; Vol 31.

Hedenquist, J.W., 1991. Boiling and dilution in the shallow portion of the Waiotapu geothermal system, New Zealand. *Geochim. Cosmochim.Acta* 55, 2753–2765.

Kilias, A., Falalakis, G., Sfeikos, A., Papadimitriou, E., Vamvaka, A., Gkarlaouni, C., 2013. The Thrace basin in the Rhodope province of NE Greece – A tertiary supradetachment basin and its geodynamic implications. *Tectonophysics* 595–596, 90–105

Meinhold, G. & Kostopoulos, D.K., 2013. The Circum-Rhodope Belt, northern Greece: Age, provenance, and tectonic setting. *Tectonophysics*, 595–596, 55–68

Roedder, E., 1984. Fluid inclusions. *In Reviews in Mineralogy, Mineralogical Society of America: Chantilly, VA, USA*, Vol 12, 644.

Sanders, J. V., 1964. Color of precious opal. Nature, 204(4964), 1151.

Shepherd, T., Rankin, A., Alderton, D., 1985. A Practical Guide to Fluid Inclusion Studies. *Blackie and Son, Glasgow, UK*.

Sillitoe, R.H., 1985. Ore-Related Breccias in Volcanoplutonic Arcs, *Economic Geology 80(6)*, 1467-1514

Sokoutis, D., Brun, J.P., Van Den Driessche, J. & Pavlides, S., 1993. A major Oligo-Miocene detachment in southern Rhodope controlling north Aegean extension, *Journal of the Geological Society*, 150, 243-246

Stewart, A.M., Chadderton, L. T. & Senior, B.R., 2010. Self-assembly in the growth of precious opal. *Journal of Crystal Growth* 312, 391–396

Tarantola, A., Diamond, L.W., Stünitz, H., 2010, Modification of fluid inclusions in quartz by deviatoric stress I: Experimentally induced changes in inclusion shapes and microstructures. *Contrib. Mineral. Petrol*, 160, 825–843.

Voudouris, P., Melfos, V., Mavrogonatos, C., Tarantola, A., Götze, J., Alfieris, D., Maneta, V., Psimis, I., 2018. Amethyst Occurrences in Tertiary Volcanic Rocks of Greece: Mineralogical, Fluid Inclusion and Oxygen Isotope Constraints on Their Genesis. *Minerals, 8, 8, 324, doi:10.3390/min8080324*.